Journal of
Synchrotron
Radiation

ISSN 0909-0495

Received 5 July 2011
Accepted 7 November 2011

A scanning Kelvin probe for synchrotron investigations: the *in situ* detection of radiation-induced potential changes

Bekir Salgin,[a]* Dirk Vogel,[a] Diego Pontoni,[b] Heiko Schröder,[c] Bernd Schönberger,[a] Martin Stratmann,[a] Harald Reichert[b,c] and Michael Rohwerder[a]

[a]Max-Planck-Institut für Eisenforschung GmbH, Max-Planck-Strasse 1, 40237 Düsseldorf, Germany, [b]European Synchrotron Radiation Facility, BP 220, 38043 Grenoble, France, and [c]Max-Planck-Institut für Metallforschung, Heisenbergstrasse 3, 70569 Stuttgart, Germany. E-mail: salgin@mpie.de

A wide range of high-performance X-ray surface/interface characterization techniques are implemented nowadays at every synchrotron radiation source. However, these techniques are not always 'non-destructive' because possible beam-induced electronic or structural changes may occur during X-ray irradiation. As these changes may be at least partially reversible, an *in situ* technique is required for assessing their extent. Here the integration of a scanning Kelvin probe (SKP) set-up with a synchrotron hard X-ray interface scattering instrument for the *in situ* detection of work function variations resulting from X-ray irradiation is reported. First results, obtained on bare sapphire and sapphire covered by a room-temperature ionic liquid, are presented. In both cases a potential change was detected, which decayed and vanished after switching off the X-ray beam. This demonstrates the usefulness of a SKP for *in situ* monitoring of surface/interface potentials during X-ray materials characterization experiments.

Keywords: Kelvin probe; radiation damage; reflectivity; surface charging.

1. Introduction

The use of synchrotron light in surface science enables the high-resolution experimental determination of the atomic and electronic structure of surfaces (or interfaces) and their interactions with adsorbates leading to the formation of new interfaces (Bachrach, 1992). To date, high-performance versions of a wide range of X-ray surface/interface characterization techniques (Mukerjee *et al.*, 1995; Stohr *et al.*, 1982; Whelan *et al.*, 1999; Mullins *et al.*, 1998; Terry *et al.*, 2002; Carbone *et al.*, 2000; Porzio *et al.*, 2011; Thomsen-Schmidt *et al.*, 2004; Heiler *et al.*, 2000; Ynzunza *et al.*, 1999) are implemented at synchrotrons.

However, these techniques are not strictly classified as 'non-destructive' owing to possible beam-induced permanent (*i.e.* damage) or reversible changes occurring during the irradiation (McGeehan *et al.*, 2007; Tremsin *et al.*, 2001). Many authors reported side-effects on the structural (Yano *et al.*, 2005; Cheng & Caffrey, 1996), chemical (Cheng & Caffrey, 1996; Weik *et al.*, 2000) and electronic properties (Lauer & Shohet, 2005; Ren *et al.*, 2010) of the materials during their synchrotron-based measurements.

As many of these effects are at least partially reversible, such as, for example, simple charging effects at interfaces and surfaces, *ex situ* analysis after the synchrotron experiment is not sufficient for the evaluation of the possible extent of beam-induced artifacts on the measurement. Hence, a suitable *in situ* method is required to provide information about any possible beam-induced changes during synchrotron experiments such as, for example, grazing-incidence X-ray scattering or X-ray reflectivity. The Kelvin probe method is a completely non-intrusive technique capable of detecting tiny changes in electrical properties of surfaces, which may be altered by electronic charging or slight structural changes that cause changes in the dipole potential. First proposed in 1898 (Kelvin, 1898), the instrumentation and the application areas of the technique broadened during the following century (Zisman, 1932; Surplice & Darcy, 1970; Baumgartner & Liess, 1988; Baikie *et al.*, 1991; Yee *et al.*, 1991). This method is also capable of detecting dipole potential changes at buried interfaces, even if the top layer is insulating (Hausbrand *et al.*, 2008) or the electronic equilibrium between the layers is disrupted, for example, by an interfacial insulator film (Rohwerder, Duc & Michalik, 2009; Rohwerder *et al.*, 2011).

Hence, the Kelvin probe technique is a very promising method for detecting radiation-induced changes. The combination of Kelvin probe with synchrotron methods dates back to the 1990s with, for example, studies of the large surface

photovoltage effects which are induced by synchrotron light on semiconducting materials such as GaAs (Mao, Kahn *et al.*, 1992; Mao, Santos *et al.*, 1992; Mao *et al.*, 1990, 1991) and GaP(110)/Ag surfaces (Chiaradia *et al.*, 1993). In these studies, however, the potential changes during irradiation were monitored only by single point measurements. In a more recent study, a direct correlation of the *ex situ* measured surface potential (after exposure) and the charge-accumulated synchrotron vacuum ultraviolet (VUV) irradiation was demonstrated on various dielectric materials (Ren *et al.*, 2010; Lauer & Shohet, 2005). Moreover, the variations in the potential during VUV irradiation were calculated by Monte Carlo simulation and were found to be in agreement with the Kelvin probe measurements (Upadhyaya *et al.*, 2005). This shows that a Kelvin probe capable of mapping *in situ* the radiation-affected zone during a synchrotron experiment would be an extremely useful tool.

In this work we report the successful integration of a scanning Kelvin probe (SKP) system with the high-energy X-ray scattering beamline ID15A (Reichert *et al.*, 2003) of the European Synchrotron Radiation Facility (ESRF, Grenoble, France). The SKP is assembled within a humidity-controlled chamber and provides two-dimensional potential maps of surfaces and/or buried interfaces during synchrotron investigations of, for example, electrochemical systems and biomimetic interfaces.

2. Experimental set-up

The SKP set-up was installed at the high-energy X-ray beamline ID15A of the ESRF for which detailed information can be found elsewhere (Reichert *et al.*, 2003; Venturini *et al.*, 2011).

The Kelvin probe is a vibrating capacitor-based technique for detecting the work function, *i.e.* the Volta potential difference between probe and sample, by measuring the vibration-induced displacement current. For minimizing stray capacities and in order to ensure a high-quality signal, it is important that the SKP tip extremity and the probed sample area form as close a perfect plate capacitor as possible (Rohwerder & Turcu, 2007). In the experiments that will be shown below, this was achieved by using an electrochemically etched needle of cylindrical corrosion-resistant Ni/Cr (80/20 wt%) alloy as the probe. The tip of the needle was cut and polished to yield a ∼300 µm-diameter flat round surface perpendicular to the shaft. Such a tip forms a sufficiently good plate capacitor configuration if the distance between the probed interface and the needle extremity is ∼50 µm. The diameter of the probe sets the achievable lateral resolution on the surface. Higher resolution down to a few micrometres is in principle possible with this Kelvin probe set-up, but with decreasing diameter of the probe the operation becomes increasingly more difficult.

In order to create a harmonic AC displacement current between probe and sample, the capacitance is varied by applying a sinusoidal mechanical oscillation to the vertical of the position needle. This vertical tip oscillation is induced by an electromagnet which is connected to a 1 kHz frequency synthesizer (G1) (Fig. 1). The current, measured at the isolated needle, is amplified and converted (current-to-voltage) by the pre-amplifier. In order to minimize a possible radiation-induced signal disturbance, the pre-amplifier is shielded. The converted signal is fed to a lock-in amplifier (LIA1) (Princeton Applied Research, Model 2510). An integrator regulates a backing voltage until the Kelvin probe signal disappears (zeroing of the displacement current). The voltage zeroing the signal equals the contact potential difference between the probe and the surface under investigation. In this way the work function difference between probe and sample is obtained at each measured point.

The response time of the circuit is between 1 and 5 s, depending on the signal-to-noise ratio. The lateral (x, y) positioning of the needle above the surface is controlled by PI (Physik Instrumente GmbH, M-227.25) high-resolution linear actuators providing a linear motion range of up to 25 mm with

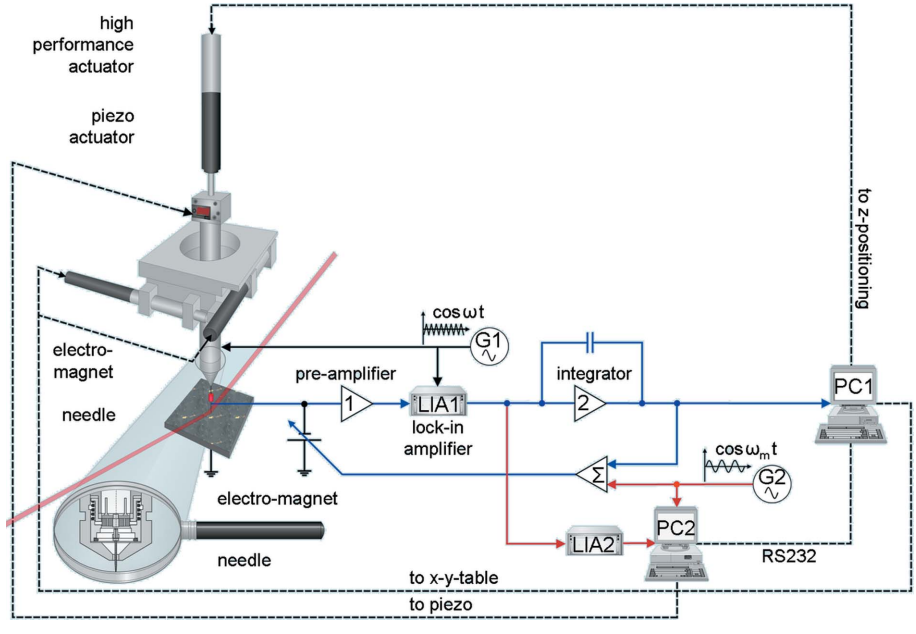

Figure 1
Operating mode of the SKP. The blue circuit shows that the frequency synthesizer G1 transmits a 1 kHz signal to the electromagnet and receives a response signal from the isolated needle, amplified by the pre-amplifier (1). A phase shifting of this signal is compensated by lock-in amplifier LIA1. The integrator (2) regulates a balancing voltage until the amplitude of the needle signal is cleared to zero. The required voltage is converted into the SKP signal by the computer PC1. The height control is achieved by a second modulation. For this an additional electronic control circuit, shown in red, consisting of frequency generator (G2), lock-in amplifier (LIA2) and PC2, is set to keep the electrical capacitance between the SKP tip and the investigated interface constant, which corresponds to keeping the distance between them constant.

submicrometre resolution. The lateral motion capability of the instrument allows two-dimensional mapping of potentials both in the regions that are directly exposed to the X-ray beam (the typical lateral beam size is 20 µm) and in regions that are macroscopically distant (mm or cm) from the X-ray beam footprint. The mechanical control of the vertical position (z-axis) is regulated by a piezo translator (Piezosystem Jena GmbH, PU90 series) in combination with a stepping motor (Physik Instrumente GmbH, M-235.5.DG). In order to keep the needle-to-sample distance constant, an additional electronic control circuit, shown in red in Fig. 1, keeps the average capacitance current constant (Wapner *et al.*, 2005; Nabhan *et al.*, 1994). This second modulation originates from a second frequency generator (G2) that transmits a 10 Hz signal at a chosen needle–sample distance. The response to this signal is detected by a second lock-in amplifier (LIA2) and computer (PC2). The fine z-positioning of the needle, as a function of the response signal, is realised by the piezo translator that is connected to a voltage amplifier (Piezosystem Jena GmbH, NV 40/1CLE). This system is regulating the average capacitance and thus the height of the needle at each new lateral step of the scan. In addition to needle positioning actuators, an xy table translation device (HUBER Diffraktionstechnik GmbH, 5102.10 series) renders the sample movements completely independent from both tip and beam positions. This allows for, for example, a rapid comparison between the potential of a fresh sample region and that of the X-ray irradiated spot during the initial alignment of radiation-sensitive samples. For increased portability of the SKP set-up, an additional double tilt stage (HUBER Diffraktionstechnik GmbH, 5203.10 series) allows the fine angular alignment of the sample surface regardless of the availability of tilt stages in the X-ray instrument.

The ambient humidity at the interior of the hermetically sealed sample chamber is monitored by a sensor (GE Measurement & Control Solutions, Series 35) capable of determining the dew point with a ± 2 K accuracy. A feedback system controls automatically the ratio of dry and humid air streams entering the chamber in order to maintain the ambient humidity at a set point. X-rays traverse thick Kapton windows that are in ohmic contact with the grounded stainless steel body of the chamber (Fig. 2). This eliminates possible X-ray charging-induced disturbances of the SKP signal. Dry air, introduced directly or after passing through water-filled bottles, is used to adjust the desired humidity level in the sample chamber.

In the following, first experiments carried out with this set-up are presented. An α-Al_2O_3 single-crystal [sapphire, (0001)-oriented] (Saint-Gobain Crystals, 10 × 10 × 0.5 mm) sample with near-atomic smoothness was used as a model substrate. As an example of the effect of the hard X-ray radiation on a solid–liquid interface, FAP-based room-temperature ionic liquid (RTIL) on sapphire was investigated {cation: 1-butyl-1-methylpyrrolidinium; $[FAP]^-$: tris(pentafluoroethyl)trifluorophosphate anion, in high-purity grade with both water and chloride content specified below 100 p.p.m., from Merck KGaA; prepared as a small droplet on the sapphire sample}. In order to ensure clean, well defined and reproducible interfaces, a rigorous preparation protocol, consisting of immersion in different solvents (acetonitrile, 2-propanol, acetone, chloroform) in an ultrasonic bath for 15 min each, 1 min piranha (H_2SO_4:H_2O_2 3:1) etching, rinsing with water, drying under argon and 30 min UV/ozone surface cleaning, was applied.

3. Examples of application: beam-induced charging at the free surface of bare sapphire and at a buried RTIL/sapphire interface

As a first example of the effect of the X-ray irradiation, the *in situ* measurement of a sapphire single crystal with (0001) surface orientation was performed. The focused monochromatic X-ray beam (E = 72.5 keV) with a flux of ∼5 × 10^{10} photons s^{-1} (beam size 5 × 20 µm at the sample position) was positioned such that it impinged on the sapphire surface in a grazing-angle geometry. The incident angle α_i varied between 0 and 1.1°. The sapphire surface was exposed to

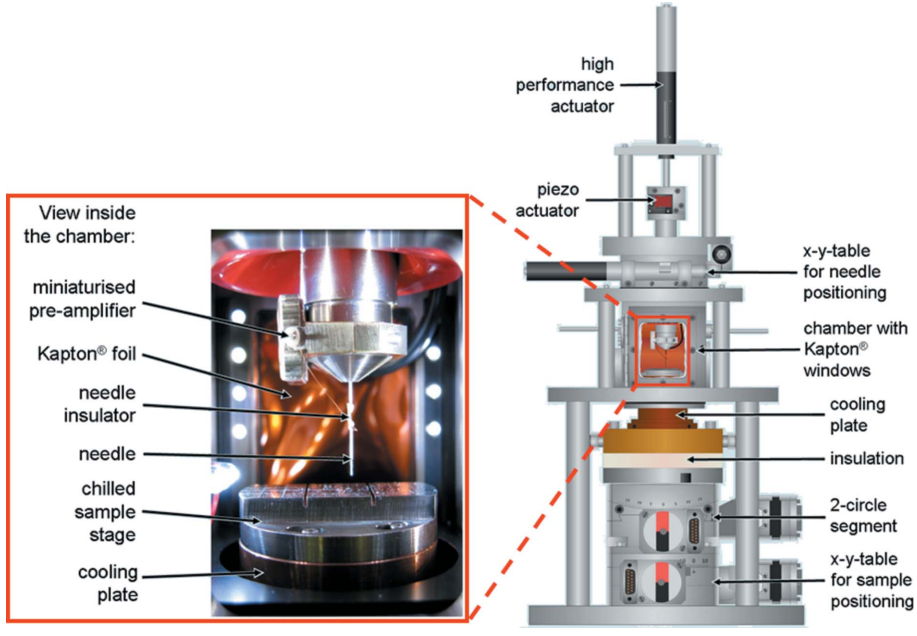

Figure 2
Sketch of the SKP instrument. Left side: view inside the chamber. The miniaturized and shielded pre-amplifier ensure a high signal-to-noise ratio. The cooling plate below the sample stage enables temperature-controlled measurements of potential changes during superficial and/or interfacial melting of solids (not shown here). The X-ray beam enters and exits the chamber through metalized Kapton windows. Right side: side view of the SKP instrument. Two separate XY motor stages allow translation with respect to the fixed X-ray beam for both the needle and sample independently.

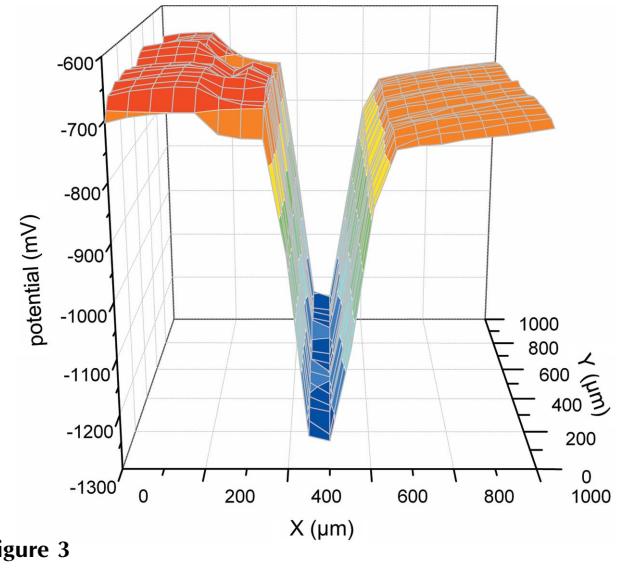

Figure 3
Potential map of a sapphire (0001) single-crystal surface during X-ray irradiation. In this representation the X-ray beam is passing through the centre of the *x*-axis and is parallel to the *y*-axis.

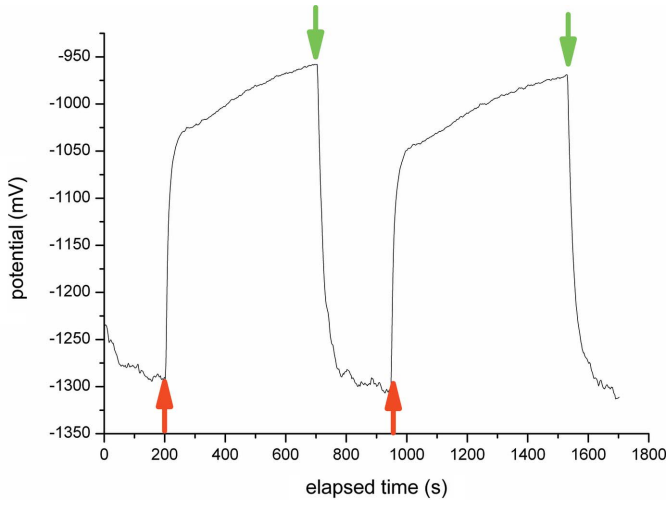

Figure 4
Point measurement of the potential at a spot lying within the X-ray irradiated footprint. Black and grey arrows (red and green online) indicate the switching off and on of the beam, respectively.

X-rays along the entire substrate length (10 mm) for incidence angles lower than ∼0.03°. At larger angles the X-ray footprint length decreased progressively down to a minimum of ∼0.26 mm at the highest $\alpha_i = 1.1°$. The Kelvin probe scanned across the region exposed to the X-rays. The tip was never directly hit by the beam during the scans because the tip-to-surface separation (typically 50 µm) was approximately one order of magnitude larger than the vertical X-ray beam size (∼5 µm). Two-dimensional potential maps covering an area of 1 × 1 mm were acquired with a 50 µm resolution on both axes. A typical potential map is presented in Fig. 3, where the X-ray beam is parallel to the *y*-axis and positioned in the centre of the *x*-axis. In the irradiated surface zone a line-shaped potential decrease of ∼550 mV is observed. Such a decrease, which is absent in the left and right regions that are not directly exposed to the X-ray beam, indicates uncompensated positive charges, resulting in an apparent decrease in the work function (Rohwerder, Isik-Uppenkamp & Stratmann, 2009). This is in agreement with the expectation that the high-energy radiation leads to photoemission of electrons, leaving a positively charged sample surface. Potential maps recorded at various times after the start of the X-ray irradiation confirmed that the potential well is localized and stationary, and it does not extend into the adjacent non-irradiated areas even after long and continuous (∼1 h) X-ray exposures.

Switching off the X-ray beam results in slow discharging of the irradiated surface region back to the original state. This can be seen in Fig. 4, which shows the temporal evolution of the potential at a spot chosen along the X-ray footprint. The black and grey arrows (red and green online) point to the times at which the beam was switched off and switched on, respectively. Fig. 4 shows that the potential is decreasing when the beam is on (t = 700–950 s) and starts to increase immediately after switch-off ($t \simeq$ 200–700 s and ∼950–1550 s). When the beam is off, the potential recovery occurs in two steps. The first part of the potential increase (∼250 mV) completes within a few seconds immediately after switching off the X-ray beam, within the response time of the Kelvin probe. This first fast recovery phase is attributed to the recombination of free electrons created by the X-ray beam above the surface with uncompensated positive charges in the sapphire insulator. The second regime, longer in time and smaller in amplitude, follows an exponential behaviour. This effect is fully reversible as can be seen from the reproducibility of the potential change upon repetition of the beam switch-on and switch-off cycle.

Similar experiments were performed in order to investigate the effects of X-ray irradiation on a buried interface between the sapphire substrate and a 420 µm-thick droplet of RTIL deposited onto it (Fig. 5). During the measurements the gap between the SKP tip and the surface of the RTIL droplet was 60 µm, while the separation between the tip and the buried

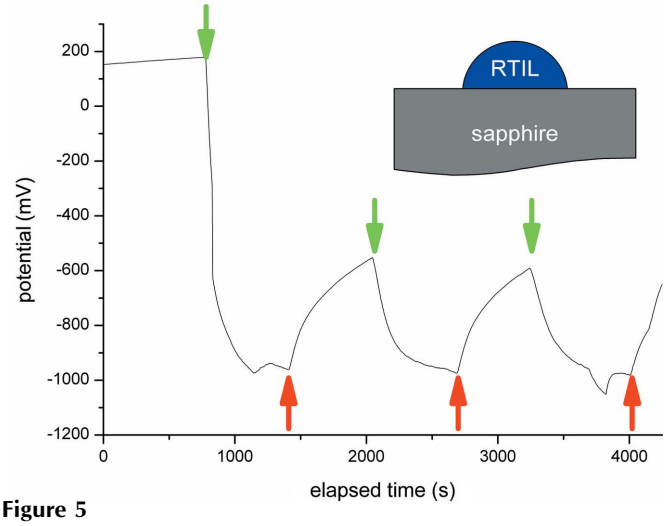

Figure 5
Point measurement of the interface potential at an irradiated spot of the RTIL/sapphire (0001) interface. Black and grey arrows (red and green online) indicate the switching-off and on of the incident beam, respectively.

RTIL/sapphire interface was 480 μm. The focused X-ray beam (vertical beam height 5 μm) was adjusted such that it impinged at a grazing angle on the surface of the sapphire. Owing to the shallow incidence angles employed, the X-ray beam traversed the RTIL droplet in regions that were far from its top, near to which the SKP tip was positioned. In such a configuration, no X-ray-induced potential changes are expected at the free surface of the RTIL droplet lying in the vicinity of the SKP tip. Contrary to this expectation, the time-resolved measurement presented in Fig. 5 demonstrates a decrease of interface potential that is even more pronounced than that observed at the free sapphire surface. The observed potential decrease is related to phenomena taking place at the buried RTIL/sapphire interface, as found for example in SKP studies of dipole potential variations in electrochemical systems (Rohwerder & Turcu, 2007). Hence, the potential change that is seen here is caused by a change in dipole potential at the interface between the sapphire and the RTIL. In such systems the substrate charges are compensated by counterions that are dissolved in the electrolyte thus forming an electrochemical double layer at the substrate–electrolyte interface. In this case the interface potential variations are related to the formation of the electrical double layer, rather than to the presence of uncompensated charges at the substrate surface, and therefore the measured decrease of interface potential reflects directly a decrease in the electrode potential, which signifies a *negative* charging of the substrate (Rohwerder & Turcu, 2007). It is still unclear why at the RTIL/sapphire interface the X-ray beam causes a negative charging of the sapphire surface. This charging plays a decisive role in the spatial arrangement of the ions in the RTIL in the vicinity of the sapphire surface (Mezger *et al.*, 2008).

The three switch on–off cycles shown in Fig. 5 (t = 0–4000 s) demonstrate that the potential reversibly decreases (increases) when the beam is switched on (off). In contrast to the situation at the bare sapphire surface, the recovery of the potential is more sluggish and does not exhibit two different time scales. The main difference is that at the buried RTIL/sapphire interface the first fast recovery process is not observed, presumably owing to the absence of mobile free electrons. It has to be pointed out here that the charge densities at buried interfaces involving an electrochemical double layer are much higher than those associated with uncompensated charges at the free surface of an insulator showing a similar potential decrease. This may be one reason for the observed difference in the decay curves. In an electrochemical system one of the main pathways for potential relaxation is represented by electrochemical reactions, *i.e.* electron transfer reactions taking place at the substrate/electrolyte interface and causing the discharging of the electrode. As sapphire is an insulator, however, the rates for this pathway are expected to be negligible.

The first results presented above demonstrate that the Kelvin probe is an extremely sensitive tool for detecting X-ray irradiation effects on surfaces and buried interfaces at their initial stages, well before they reach the level of irreversible structural damage. The observed surface/interface charging effects determine potential variations that remain within a 1 V range. The discharging phenomena detected after switching off the X-ray beam are related to the fact that even at insulating surfaces and interfaces the charges retain a certain degree of mobility. The observed magnitudes of the potential variations are, however, sufficiently large to have a significant impact on the structural details of the surfaces/interfaces under X-ray investigation. For example, the orientation of molecules at buried solid/liquid interfaces can be altered by interface potential changes of 0.1 V. Conversely, the adsorption of molecules induces surface or dipole potential variations of typically 0.25 V (Bewig & Zisman, 1964), and up to $\sim$1 V in extreme cases (Young & Crowell, 1962). Preliminary studies of the effect of varying the intensity of the X-ray beam suggest that for each specific sample it is possible to find an optimal irradiation intensity allowing meaningful structural results under conditions of minimal interface charging. A comprehensive study of the effects of the X-ray beam energy and intensity will be presented elsewhere.

4. Conclusions

A Kelvin probe set-up has been integrated at a synchrotron beamline. The *in situ* combination of spatially resolved Kelvin probe measurements with X-ray scattering techniques allows the structural and electronic properties of a wide class of interfaces to be probed simultaneously. This novel combination of techniques provides the unique ability to discriminate X-ray beam-induced effects from intrinsic materials properties. We observed charging effects at the X-ray irradiated zone both at free surfaces and at buried interfaces. On a bare sapphire substrate, localized positive charging of the surface has been detected. This effect is attributed to the ejection of photoelectrons, resulting in a decrease of the measured potential owing to an apparent decrease of the work function. When the beam is switched off, the positive excess charge in the irradiated zone is compensated in a two-step process. In the case of a buried RTIL/sapphire interface, representing a wide class of electrochemical systems, we instead observed a *negative* sapphire charging. This effect, which is not fully understood yet and requires further investigation, has a profound effect on the structure of RTILs at this buried interface (Mezger *et al.*, 2008).

References

Bachrach, R. Z. (1992). *Synchrotron Radiation Research: Advances in Surface and Interface Science*, Vol. 1, *Techniques*, edited by R. Z. Bachrach, pp. 1–54. New York: Plenum Press.

Baikie, I. D., Mackenzie, S., Estrup, P. J. Z. & Meyer, J. A. (1991). *Rev. Sci. Instrum.* **62**, 1326–1332.

Baumgartner, H. & Liess, H. D. (1988). *Rev. Sci. Instrum.* **59**, 802–805.

Bewig, K. W. & Zisman, W. A. (1964). *J. Phys. Chem.* **68**, 1804–1813.

Carbone, M., Bobrov, K., Comtet, G., Dujardin, G. & Hellner, L. (2000). *Surf. Sci.* **467**, 49–57.

Cheng, A. & Caffrey, M. (1996). *Biophys. J.* **70**, 2212–2222.

Chiaradia, P., Bonnet, J. E., Fanfoni, M., Goletti, C. & Lampel, G. (1993). *Phys. Rev. B*, **47**, 13520–13526.

Hausbrand, R., Stratmann, M. & Rohwerder, M. (2008). *J. Electrochem. Soc.* **155**, C369–C379.
Heiler, M., Chasse, A., Schindler, K. M., Hollering, M. & Neddermeyer, H. (2000). *Surf. Sci.* **454**, 36–40.
Kelvin, L. (1898). *Philos. Mag.* **46**, 82.
Lauer, J. L. & Shohet, J. L. (2005). *IEEE Trans. Plasma Sci.* **33**, 248–249.
McGeehan, J. E., Carpentier, P., Royant, A., Bourgeois, D. & Ravelli, R. B. G. (2007). *J. Synchrotron Rad.* **14**, 99–108.
Mao, D., Kahn, A., Lelay, G., Marsi, M., Hwu, Y. & Margaritondo, G. (1992). *Appl. Surf. Sci.* **56**, 142–150.
Mao, D., Kahn, A., Lelay, G., Marsi, M., Hwu, Y., Margaritondo, G., Santos, M., Shayegan, M., Florez, L. T. & Harbison, J. P. (1991). *J. Vac. Sci. Technol. B*, **9**, 2083–2089.
Mao, D., Kahn, A., Marsi, M. & Margaritondo, G. (1990). *Phys. Rev. B*, **42**, 3228–3230.
Mao, D., Santos, M., Shayegan, M., Kahn, A., Lelay, G., Hwu, Y., Margaritondo, G., Florez, L. T. & Harbison, J. P. (1992). *Phys. Rev. B*, **45**, 1273–1283.
Mezger, M., Schröder, H., Reichert, H., Schramm, S., Okasinski, J. S., Schöder, S., Honkimäki, V., Deutsch, M., Ocko, B. M., Ralston, J., Rohwerder, M., Stratmann, M. & Dosch, H. (2008). *Science*, **322**, 424–428.
Mukerjee, S., Srinivasan, S., Soriaga, M. P. & McBreen, J. (1995). *J. Electrochem. Soc.* **142**, 1409–1422.
Mullins, D. R., Overbury, S. H. & Huntley, D. R. (1998). *Surf. Sci.* **409**, 307–319.
Nabhan, W., Broniatowski, A., Derosny, G. & Equer, B. (1994). *Microsc. Microanal. Microstruct.* **5**, 509–517.
Porzio, W., Scavia, C., Barba, L., Arrighetti, G. & Milita, S. (2011). *Eur. Polym. J.* **47**, 273–283.
Reichert, H., Honkimaki, V., Snigirev, A., Engemann, S. & Dosch, H. (2003). *Physica B*, **336**, 46–55.
Ren, H., Sinha, H., Sehgal, A., Nichols, M. T., Antonelli, G. A., Nishi, Y. & Shohet, J. L. (2010). *Appl. Phys. Lett.* **97**, 072901.
Rohwerder, M., Duc, L. & Michalik, A. (2009). *Electrochim. Acta*, **54**, 6075–6081.
Rohwerder, M., Isik-Uppenkamp, S. & Amarnath, C. A. (2011). *Electrochim. Acta*, **56**, 1889–1893.
Rohwerder, M., Isik-Uppenkamp, S. & Stratmann, M. (2009). *Electrochim. Acta*, **54**, 6058–6062.
Rohwerder, M. & Turcu, F. (2007). *Electrochim. Acta*, **53**, 290–299.
Stohr, J., Jaeger, R. & Brennan, S. (1982). *Surf. Sci.* **117**, 503–524.
Surplice, N. A. & Darcy, R. J. (1970). *J. Phys. E*, **3**, 477–482.
Terry, J., Schulze, R. K., Farr, J. D., Zocco, T., Heinzelman, K., Rotenberg, E., Shuh, D. K., Van der Laan, G., Arena, D. A. & Tobin, J. G. (2002). *Surf. Sci.* **499**, L141–L147.
Thomsen-Schmidt, P., Hasche, K., Ulm, G., Herrmann, K., Krumrey, M., Ade, G., Stumpel, J., Busch, I., Schadlich, S., Schindler, A., Frank, W., Hirsch, D., Procop, M. & Beck, U. (2004). *Appl. Phys. Mater. Sci. Process.* **78**, 645–649.
Tremsin, A. S., Pearson, J. F., Nichols, A. P., Owens, A., Brunton, A. N. & Fraser, G. W. (2001). *Nucl. Instrum. Methods Phys. Res. A*, **459**, 543–551.
Upadhyaya, G. S., Shohet, J. L. & Lauer, J. L. (2005). *Appl. Phys. Lett.* **86**, 102101.
Venturini, F., Schöder, S., Kuhs, W. F., Honkimäki, V., Melesi, L., Reichert, H., Schober, H. & Thomas, F. (2011). *J. Synchrotron Rad.* **18**, 251–256.
Wapner, K., Schoenberger, B., Stratmann, A. & Grundmeier, G. (2005). *J. Electrochem. Soc.* **152**, E114–E122.
Weik, M., Ravelli, R. B., Kryger, G., McSweeney, S., Raves, M. L., Harel, M., Gros, P., Silman, I., Kroon, J. & Sussman, J. L. (2000). *Proc. Natl Acad. Sci. USA*, **97**, 623–628.
Whelan, C. M., Barnes, C. J., Walker, C. G. H. & Brown, N. M. D. (1999). *Surf. Sci.* **425**, 195–211.
Yano, J., Kern, J., Irrgang, K. D., Latimer, M. J., Bergmann, U., Glatzel, P., Pushkar, Y., Biesiadka, J., Loll, B., Sauer, K., Messinger, J., Zouni, A. & Yachandra, V. K. (2005). *Proc. Natl Acad. Sci. USA*, **102**, 12047–12052.
Yee, S. G., Oriani, R. A. & Stratmann, M. (1991). *J. Electrochem. Soc.* **138**, 55–61.
Ynzunza, R. X., Tober, E. D., Palomares, F. J., Wang, Z., Daimon, H., Kaduwela, A. P., Chen, Y., Hussain, Z., Van Hove, M. A. & Fadley, C. S. (1999). *Surf. Sci.* **441**, 301–310.
Young, D. M. & Crowell, A. D. (1962). *Physical Adsorption of Gases.* London: Butterworths.
Zisman, W. A. (1932). *Rev. Sci. Instrum.* **3**, 367–370.